

# Influence of partial coherent illumination on aerial image based aberration measurement of projection optics in lithographic tools

Tingting ZHOU<sup>a</sup>, Shiyuan LIU<sup>\*,b</sup>, Wei LIU<sup>a</sup>, Lijuan WANG<sup>a</sup>

<sup>a</sup> Wuhan National Laboratory for Optoelectronics, Huazhong University of Science and Technology, Wuhan, China.

<sup>b</sup> State Key Laboratory of Digital Manufacturing Equipment and Technology, Huazhong University of Science and Technology, Wuhan, China.

## ABSTRACT

In this paper, the aberration measurement technique using aerial image sensor (AIS) is further derived, and the influence of partially coherent illumination on the performance of this technique is analyzed comprehensively in practice. The AIS based technique detects the intensity of the aerial image to obtain the wavefront aberration on each sampling point of the exit pupil using a set of 36 binary gratings with different pitches and orientations. The simulation work conducted by the lithographic simulator PROLITH has demonstrated that the aberration measurement errors grow with the partial coherent factor increasing. Two effects of the partially coherent illumination are proposed to interpret such influence that causes the measurement errors.

**Keywords:** lithography, wavefront aberration metrology, aerial image sensor, Zernike, partial coherence in imaging

## 1. INTRODUCTION

With ever decreasing feature sizes and pushing the limit of optical lithography, the overall performance of the optical imaging system becomes increasingly important. Contributing to a degradation of the image quality, the wavefront aberration of the projection lens in lithographic tools plays a critical role in the overall system performance<sup>[1,2]</sup>. Usually, Zernike polynomials are introduced to represent the lens aberration, which are a complete orthogonal set of polynomials over the interior of the unit circle<sup>[3,4]</sup>. The Zernike series representation is useful as it provides explicit expressions for the well-known low order aberration such as spherical, coma, astigmatism, etc which can be detected accurately in various aberration measurement techniques. However, in order to satisfy the requirement of optical path tolerances in the condition of higher numerical aperture (NA) in the future, the measurement of the higher order coefficients of Zernike polynomials becomes a necessary prerequisite.

On the whole, a variety of in situ measurement techniques have been developed, which can be roughly classified into two types: pupil based and image based. In recent years, several pupil based techniques have been reported such as the integrated lens interferometer at scanner (ILIAS)<sup>[5]</sup>, integrated projecting optics tester (iPot)<sup>[6,7]</sup>, and in situ phase measurement interferometer (iPMI)<sup>[8]</sup>. They are generally faster and more accurate than image based techniques because of the less metrology errors. Although pupil based techniques are able to accurately retrieve aberration up to the 37<sup>th</sup> Zernike coefficient, they are integrated with complex apparatus such as embedded interferometer and micro lens array, which result in high cost for lithographic tools. On the other hand, ASML Corporation has developed an aerial image based technique known as TIS at multiple illumination settings (TAMIS)<sup>[9]</sup>, which utilizes a transmission image sensor (TIS) built into the wafer stage for receiving the aerial image intensity of the test binary marks. This measurement technique reduces the cost but maintains high sensitivity only to spherical, coma and astigmatism.

In order to exactly measure aberration up to the 37<sup>th</sup> Zernike coefficient, Nikon Corporation has proposed a Z37 aerial image sensor (AIS) technique<sup>[10-13]</sup>. It has introduced a set of 36 binary grating marks with different pitches and orientations, corresponding to 72 pupil sampling points over the pupil plane. The wavefront aberration at each sampling point can be easily obtained from the spectrum of the aerial image intensity. Since obtaining the wavefront aberration at each sampling point requires highly coherent illumination, the Z37 AIS technique works best with coherent sources. In

\* Contact author: shyliu@mail.hust.edu.cn; phone: +86 27 87792409; fax: +86 27 87792413.

practice, however, partial coherent sources are used in conventional lithographic tools which seriously affect the accuracy of the wavefront aberration measurement of the Z37 AIS technique. Therefore, it is unsuitable for aberration measurement in lithographic tools with partially coherent illumination.

In this paper, we further investigate the aberration measurement method based on aerial image sensor, and then analyze the influence of partially coherent illumination. The fundamental relationship between the aberration and the first-order spectrum of the aerial image intensity is derived and established. Several simplifications are remarked in the process of deviation. Extensive simulation work was conducted by the lithographic simulator PROLITH, and two effects of the partially coherent illumination are proposed to interpret the influence.

## 2. ABERRATION MEASUREMENT METHOD

### 2.1 Theory

The optical imaging system in lithographic tools is shown in Fig.1, in which the object plane coordinates  $(x_0, y_0)$ , image plane coordinate  $(x_i, y_i)$ , and pupil plane coordinate  $(f, g)$  are all normalized according to canonical coordinates proposed by Hopkins<sup>[14]</sup>. Thus the cut-off frequency from the pupil plane is normalized to the unit of one.

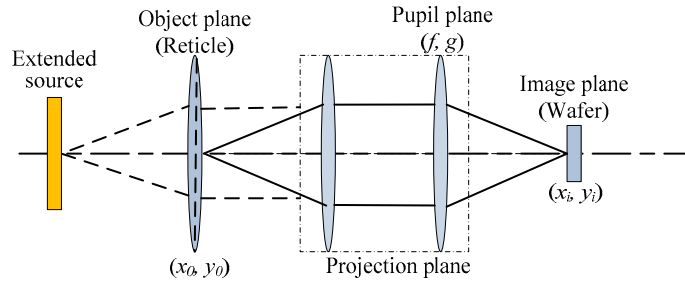


Fig.1 Optical lithographic imaging system

In this measurement method, an aerial image sensor built into the wafer stage for detecting the aerial image intensity of the reticle. The spectrum of the aerial image intensity is extracted by Fourier transformation and is subsequently analyzed for aberration measurement. This reticle is designed to be a binary grating with opening width  $p_m/2$ , where  $m = 1, 2, 3, \dots, 36$ . The orientation of the binary grating is defined by the angle  $\theta$  ranging from  $0^\circ$  to  $180^\circ$ . Considering the one-dimensional object in the  $\theta$  direction with normalized spatial period  $p_m = 1/f_m$ , the spectrum of the  $m^{\text{th}}$  grating  $O(f, g)$  becomes:

$$O(f, g) = \frac{1}{2} \text{sinc}\left(\frac{f}{2f_m}\right) \sum_{a=-\infty}^{+\infty} \delta(f - af_m), \quad a \in Z \quad (1)$$

Actually, as the even-order diffraction lights passing the binary grating are missing except the  $0^{\text{th}}$ -order diffraction light, the spectrum  $O(f, g)$  is nonzero only at odd-order frequencies and  $0^{\text{th}}$ -order frequency:  $f = 0, \pm f_m, \pm 3f_m, \dots, (2k+1)f_m, k \in N$ .

Based on the partially coherent imaging theory in the frequency domain, the aerial image intensity of the one-dimensional object can be expressed as:

$$i(x_i, y_i) = \iiint_{-\infty}^{+\infty} TCC(f', g'; f'', g'') O(f', g') O^*(f'', g'') \exp[2\pi j x_i (f' - f'') + y_i (g' - g'')] df' dg' df'' dg'' \quad (2)$$

where  $O(f', g')$  is the Fourier spectrum of the binary grating mentioned above, and  $TCC(f', f''; g', g'')$  is introduced as the concept of transmission cross-coefficient:

$$TCC(f', g'; f'', g'') = \int \int_{-\infty}^{+\infty} J(f_c, g_c) H(f' + f_c, g' + g_c) H^*(f'' + f_c, g'' + g_c) df_c dg_c \quad (3)$$

where  $J(f_c, g_c)$  represents a typical illumination source in optical lithography as:

$$J(f_c, g_c) = \frac{1}{\pi\sigma^2} \text{circ}\left(\frac{\sqrt{f_c^2 + g_c^2}}{\sigma}\right) \quad (4)$$

where  $\sigma$  is the partial coherent factor which defined as the effective source filling factor in the projection optics pupil. Optical transfer function  $H(f, g)$  is commonly introduced to describe the property of the object lens system on a certain illumination source condition:

$$H(f, g) = \text{circ}(\sqrt{f^2 + g^2}) \exp[jkW(f, g)] \quad (5)$$

where  $k = 2\pi/\lambda$  is the wave number;  $\lambda$  is the wavelength of the monochromatic light source; and  $W(f, g)$  is the total wavefront aberration including a defocus aberration  $W_{defocus}$  and a relative lens aberration  $W_{lens}$ . The latter one  $W_{lens}$  is composed of an odd aberration  $W_{odd}$  as well as an even aberration  $W_{even}$ .

In order to achieve a certain connection between the wavefront aberration and the intensity of the aerial image, Eqs.(1) to (3) are combined together. The  $n^{\text{th}}$ -odd spectrum of intensity can be expressed as:

$$\begin{aligned} I(nf_m, 0) &= C_0 [TCC(nf_m, 0; 0, 0) + TCC(0, 0; -nf_m, 0)] \\ I(-nf_m, 0) &= C_0 [TCC(-nf_m, 0; 0, 0) + TCC(0, 0; nf_m, 0)] \end{aligned} \quad (6)$$

where  $n=1, 3, 5, \dots$ , and  $C_0$  is a determined constant unrelated to the spatial period  $p_m = 1/f_m$ .

For the same order of diffraction, the terms in Eq. (2) maintain constant except the term of  $\exp[2\pi j x_i(f' - f'') + y_i(g' - g'')]$ . This means that the spectrum of the intensity is determined by  $f' - f''$  and  $g' - g''$  merely for a certain order of diffraction. So each odd-order spectrum of the aerial image intensity is considered to be the interaction between the 0<sup>th</sup>-order diffraction and each odd-order diffraction spectrum term, and it contains all the wavefront aberration information that we are interested in. Therefore, wavefront aberration can be extracted just from the first-order spectrum of the aerial image intensity, that is  $n = 1$ .

Under the nearly fully coherent illumination condition, the partial coherent factor  $\sigma$  approximates 0, and the parameters of the illumination source  $f_c, g_c$  can be also treated as 0, thus the illumination source can be normalized as:

$$\iint_S J(f_c, g_c) df_c dg_c = 1 \quad (7)$$

Replacing the  $TCC$  with the relationships in Eqs. (1), (4) and (7), Eq. (8) can be simplified as:

$$\begin{aligned} I(f_m, 0) &= C_1 [\exp(jkW(\rho, \theta)) + \exp(-jkW(\rho, \theta + \pi))] \\ I(-f_m, 0) &= C_1 [\exp(jkW(\rho, \theta + \pi)) + \exp(-jkW(\rho, \theta))] \end{aligned} \quad (8)$$

where  $C_1$  is a certain constant unrelated to the aberration and diffraction orders; the wavefront aberration  $W(\rho, \theta)$  is the normalized form of  $W(f, g)$  in the pupil plane, and  $\rho$  is the normalized radius ranging from 0 to 1.

## 2.2 Aberration measurement

Considering the property of the odd aberration and even aberration, they can be obtained separately. In terms of the symmetry of the odd aberration, there is:

$$W_{odd}(\rho, \theta) = -W_{odd}(\rho, \theta + \pi) \quad (9)$$

From Eqs.(8) and (9), the relationship between the odd aberration and the first-order spectrum can be expressed as:

$$I(f_m, 0) = 2C_1 \exp[jkW_{odd}(\rho, \theta)] \quad (10)$$

Obviously, the odd wavefront aberration is linear with the phase shift of the first-order spectrum of intensity  $\varphi$ . This is the relationship for the odd wavefront aberration measurement:

$$W_{odd}(\rho, \theta) = \frac{\varphi(f_m, \theta)}{k} \quad (11)$$

On the other hand, as shown in Fig.2, a perfect wavefront focuses on the ideal focal plane, while an aberrated wavefront comes to a plane which is called the best focal plane in which the first-order spectrum of the intensity reaches the extreme value. The axial shift between the best focal plane and the ideal focal plane is defined as the defocus  $D$ .

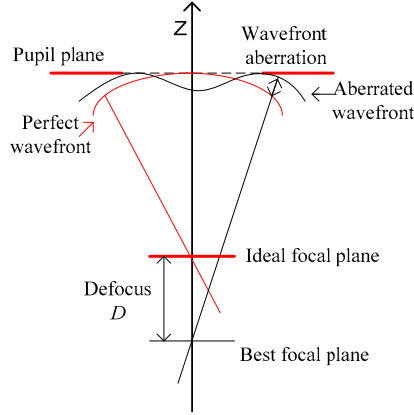


Fig.2 The defocus caused by even wavefront aberration

Based on the optical theory, the defocus aberration is another type of even aberration which can be expressed as the sum of relative even aberrations, thus the relative even aberration  $W_{even}(\rho, \theta)$  is proportional to the defocus as<sup>[15, 16]</sup>:

$$W_{even}(\rho, \theta) = -W_{defocus}(\rho, \theta) = -D\left(\sqrt{1 - NA^2 \rho^2} - 1\right) \quad (12)$$

where  $D$  (in nm) is the defocus shown in Fig.2, and  $NA$  is the image-side numerical aperture of the projection lens.

### 2.3 Zernike coefficient measurement

In this aberration measurement method, the aberrations at selected points on the lens exit pupil are obtained directly from a set of 36 binary grating objects with opening width  $p_m/2$ . They are designed with different spatial periods and in orientations such as  $\theta = 0^\circ, 30^\circ, 45^\circ, 90^\circ, 120^\circ$ , and  $150^\circ$ . Two symmetric points are detected with each binary grating by scanning the aerial image sensor each time. So the aberration up to 37<sup>th</sup> Zernike coefficient can be obtained by least-square method. The odd and even wavefront aberration can be expressed respectively:

$$\begin{bmatrix} W_{odd}(\rho_1, \theta_1) \\ W_{odd}(\rho_2, \theta_2) \\ \vdots \\ W_{odd}(\rho_{36}, \theta_{36}) \end{bmatrix} = \begin{bmatrix} R_2(\rho_1, \theta_1) & R_3(\rho_1, \theta_1) & \dots & R_{35}(\rho_1, \theta_1) \\ R_2(\rho_2, \theta_2) & R_3(\rho_2, \theta_2) & \dots & R_{35}(\rho_2, \theta_2) \\ \vdots & \vdots & \dots & \vdots \\ R_2(\rho_{36}, \theta_{36}) & R_3(\rho_{36}, \theta_{36}) & \dots & R_{35}(\rho_{36}, \theta_{36}) \end{bmatrix} \begin{bmatrix} Z_2 \\ Z_3 \\ \vdots \\ Z_{35} \end{bmatrix} \quad (13)$$

$$\begin{bmatrix} W_{even}(\rho_1, \theta_1) \\ W_{even}(\rho_2, \theta_2) \\ \vdots \\ W_{even}(\rho_{36}, \theta_{36}) \end{bmatrix} = \begin{bmatrix} R_4(\rho_1, \theta_1) & R_5(\rho_1, \theta_1) & \dots & R_{37}(\rho_1, \theta_1) \\ R_4(\rho_2, \theta_2) & R_5(\rho_2, \theta_2) & \dots & R_{37}(\rho_2, \theta_2) \\ \vdots & \vdots & \dots & \vdots \\ R_4(\rho_{36}, \theta_{36}) & R_5(\rho_{36}, \theta_{36}) & \dots & R_{37}(\rho_{36}, \theta_{36}) \end{bmatrix} \begin{bmatrix} Z_4 \\ Z_5 \\ \vdots \\ Z_{37} \end{bmatrix} \quad (14)$$

In a more compact notation, Eqs. (13) and (14) can be rewritten as:

$$\mathbf{W}_{odd}(\rho, \theta) = \mathbf{Z}_{odd} \mathbf{R}_{odd}(\rho, \theta) \quad (15)$$

$$\mathbf{W}_{even}(\rho, \theta) = \mathbf{Z}_{even} \mathbf{R}_{even}(\rho, \theta) \quad (16)$$

where  $\mathbf{W}_{odd}$  and  $\mathbf{W}_{even}$  are vectors respectively indicating the odd and even aberration at the setting of 36 binary gratings;  $\mathbf{Z}_{odd}$  and  $\mathbf{Z}_{even}$  are unknown Zernike coefficient vectors to be measured; and  $\mathbf{R}_{odd}$  and  $\mathbf{R}_{even}$  are matrices of odd and even Zernike polynomial, respectively.

### 3. SIMULATION

#### 3.1 Theoretical validation under coherent condition

The essentials of this aberration measurement are two linear relationships, between the phase shift and the odd aberration, and between the defocus and the even aberration, respectively. The lithographic simulator PROLITH was used in these simulations. The wavelength is 193nm, and the NA is 0.75. To simulate the nearly fully coherent illumination condition, we set the partial coherent factor as 0.001. The input wavefront aberration ranges from  $-8m\lambda$  to  $8m\lambda$  with an increment of  $0.5m\lambda$ . Figure 3 compares the calculated and simulated results, in which the lines show the linear relationships calculated by Eq. (11) and Eq. (12) while the points depict the relationships simulated by PROLITH.

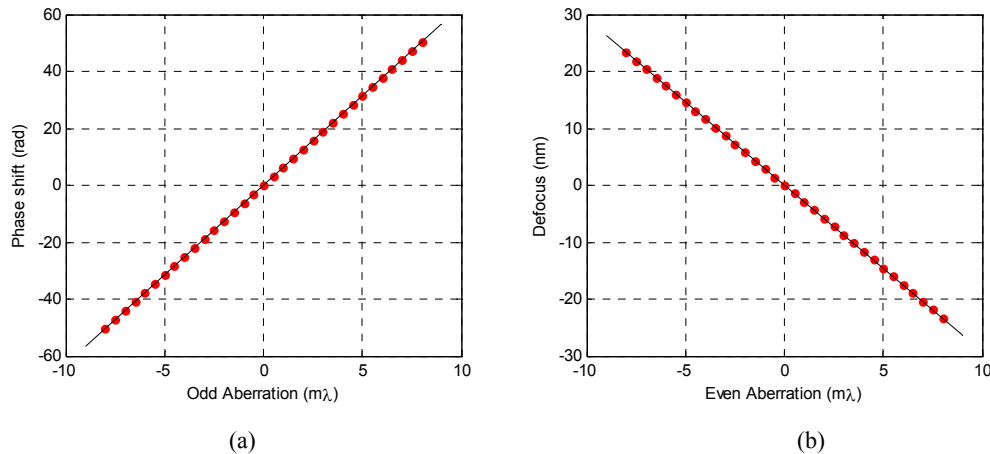


Fig.3 Correlation plots between (a) the odd aberration and the phase shift, and (b) between the even aberration and defocus. The lines are calculated by Eq. (11) and Eq. (12) while the points are simulated by PROLITH.

From the results shown in Fig.3, it is clear that the calculated values by Eqs.(11) and (12) have an excellent correlation with those simulated by PROLITH, thus the relationships in Eq. (11) and Eq. (12) are verified.

Figure 4 depicts further simulations by PROLITH to evaluate the overall performance of the proposed technique under coherent condition. Two sets of Zernike coefficients were generated to simulate the input wavefront aberrations, in which the higher-order Zernike coefficients of Input 1 are much smaller than those of Input 2, thus the simulated aberration of Input 1 is more practical as in a real-world lithographic tool.

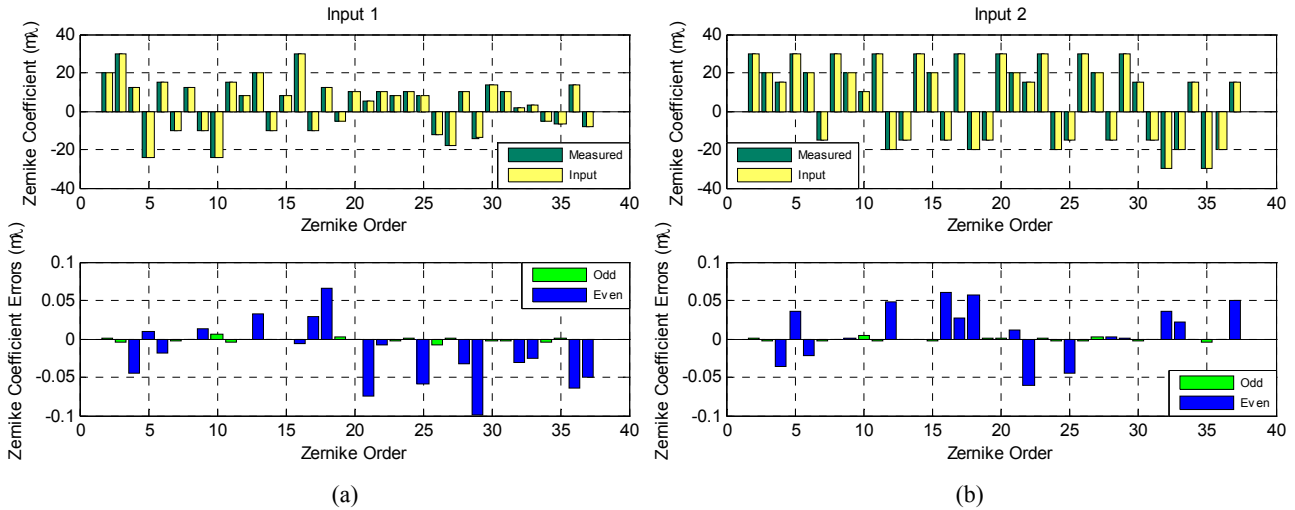


Fig.4 Two simulations of Zernike coefficient measurement under coherent condition. The wavelength is 193nm, the NA is 0.75, and the partial coherent factor is 0.001.

From Fig.4 it is noted that the absolute errors of the measured Zernike coefficients are all below  $0.1m\lambda$ , even in the case of Input 2 with large values of higher-order aberrations. These results and a lot of other simulations demonstrate that the proposed technique yields a high quality of wavefront estimate under coherent condition.

### 3.2 Influence of partial coherent factor

In practice, the illumination source of a real-world lithographic tool cannot be reduced to a point and is usually larger than 0.3. Figure 5 depicts the measurement results of some single Zernike coefficients compared to the theoretical values at different sampling points when the partial coherent factor varies from 0.05 to 0.3. As an example,  $Z_7=0.02$  is used to simulate the odd aberration, while  $Z_9=0.02$  is representative of even aberration. When the partial coherence is smaller than 0.05, it would be considered as an ideal constitution of the illumination coherence.

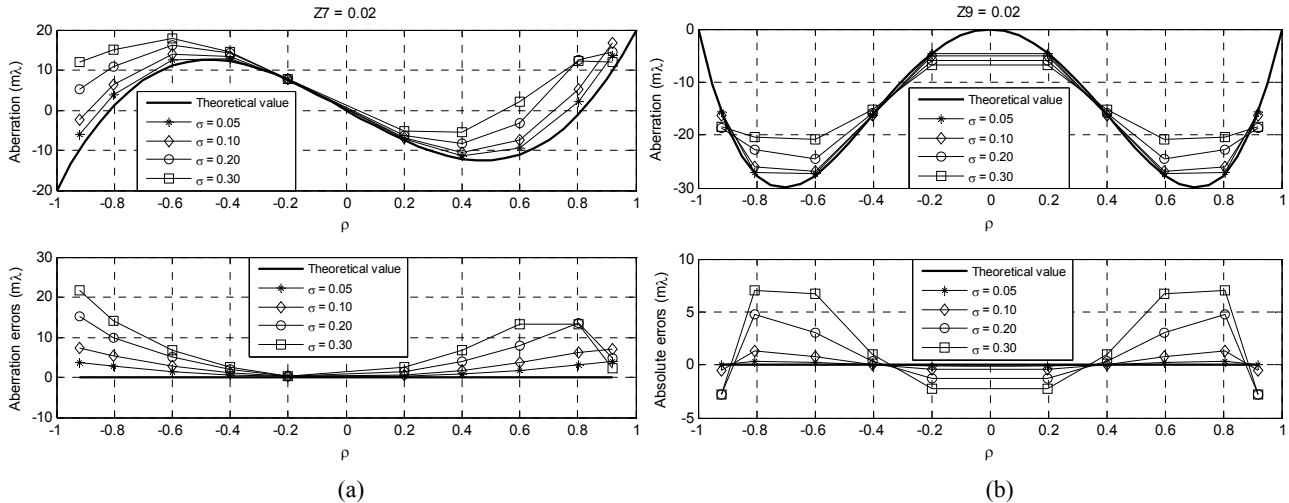


Fig.5 The variation of the measured aberration at different sampling points with partial coherence factor ranging from 0.05 to 0.3. (a)  $Z_7$  is set to be 0.02 to simulate the odd aberration, and (b)  $Z_9$  is set to be 0.02 to simulate the even aberration.

In Fig.5 it is clear that the measurement error significantly increases as the partial coherence factor  $\sigma$  grows. For instance, the root mean square (RMS) of the absolute aberration errors in Fig.5 (a) reaches  $8.013m\lambda$  when  $\sigma=0.2$ , and then becomes  $10.602m\lambda$  when  $\sigma$  grows up to 0.3. From these simulation results it is concluded that the partial coherent factor can significantly influence the measurement error.

Figure 6 shows the RMS of aberration measurement errors for different types of wavefront aberrations as the partial coherent factor changes from 0.001 to 0.4. The RMS of the aberration errors is calculated from all the values of wavefront aberrations at the sampling points shown in Fig.5. It is noted that generally the RMS of aberration measurement errors becomes larger as the partial coherent factor increases, but such influence of partial coherent factor is different for different types of aberrations.

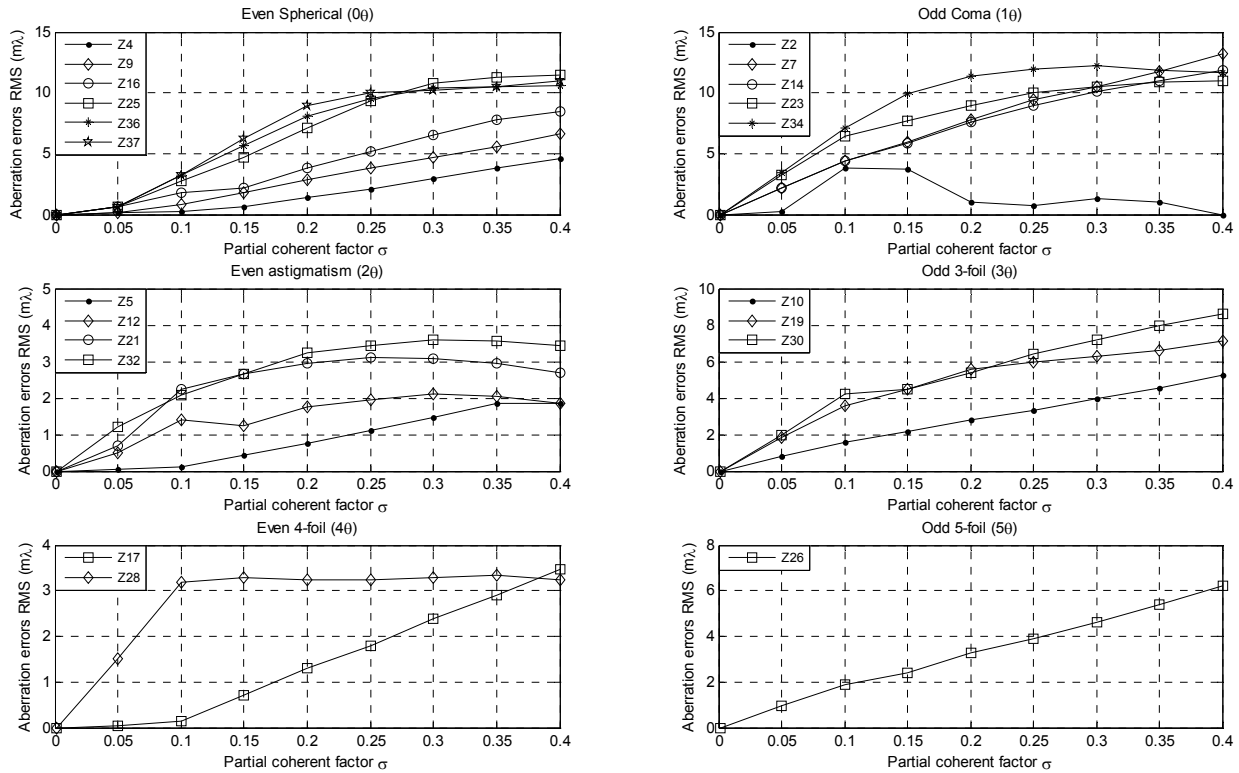


Fig.6 Influence of partial coherent factor on measurement errors for different types of aberrations.

The influence of partial coherent factor  $\sigma$  on the overall performance of aberration measurement was also simulated as shown in Fig.7 and Fig.8, in which  $\sigma$  is set to be 0.1, 0.2, 0.3 and 0.4, and all the inputs of Zernike coefficients are the same as Input 1 shown in Fig.4. As expected, the measurement errors of Zernike coefficients increase as  $\sigma$  increases.

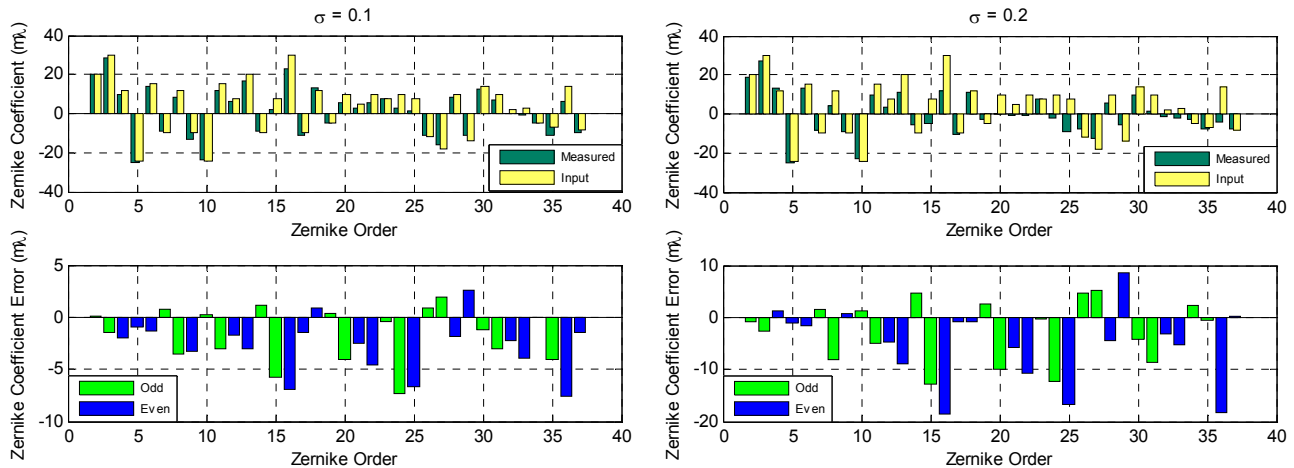


Fig.7 Overall performance of measuring aberrations up to 37th Zernike coefficient with partial coherent factor  $\sigma$  is 0.1 and 0.2.

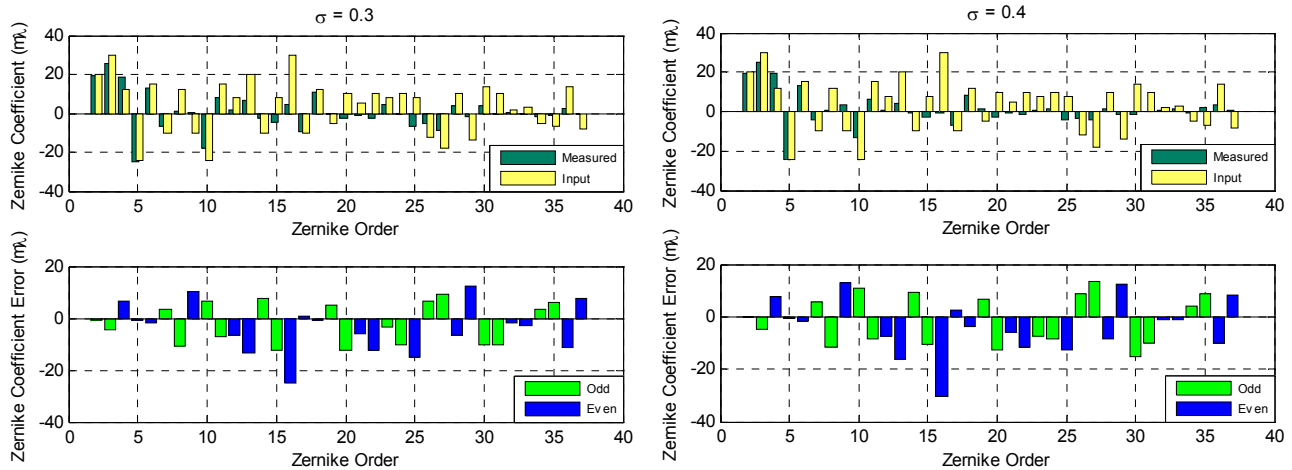


Fig.8 Overall performance of measuring aberrations up to 37th Zernike coefficient with partial coherent factor  $\sigma$  is 0.3 and 0.4.

## 4. INTERPRETATION

### 4.1 Effect of diffraction spot

From the simulation results, the partial coherent factor has a significant influence on the accuracy of the aberration measurement method. Noting that several simplifications have been introduced in the mathematical derivation, here we propose two effects of partial coherent factor to try to interpret the above influence. One effect is that the off-axis outer parts of the illumination source with a finite size may cause the first diffraction orders to pass outside the lens pupil. In Eq. (7), we calculate the integration of illumination source as 1 under the fully coherent condition. Under the partial coherent condition, however, the area of the integration would be less than 1 if the first-order diffraction light is too close to the boundary of the pupil, or even part of the first-order diffraction light exceeds the pupil. In this case, the difference of the integral area contributes to the error of aberration measurement.

In order to reduce the measurement error, the integral region  $S$  in Eq. (7) should be calculated as the intersection of the pupil function in Eq. (5) and illumination source in Eq. (4), shown as the shadowed area in Fig.9. Here  $R_1$  represents the radius of the first-order diffraction spot which is equal to the partial coherent factor  $\sigma$ ,  $R_2$  is the radius of the exit pupil, and the distance of these two centers of circles is equal to the normalized grating pitch.

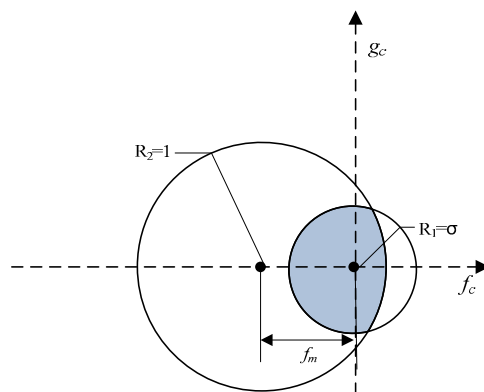


Fig.9 Representation of the integral region  $S$

## 4.2 Effect of aberration smoothness

The other effect is that the wavefront aberration at each sampling point is simply assumed to be the smoothed average value of those inside the integral region  $S$ . From Eq. (6), the first-order spectrum of intensity is expressed as:

$$\begin{aligned} I(nf_m, 0) = & C_0 \iint_S J(f_c, g_c) \exp\{jk[W(f_m + f_c, g_c) - W(f_c, g_c)]\} df_c dg_c \\ & + C_0 \iint_S J(f_c, g_c) \exp\{jk[W(f_c, g_c) - W(-f_m + f_c, g_c)]\} df_c dg_c \end{aligned} \quad (17)$$

Considering the wavefront aberration is extremely small, we simplify the expressions as:

$$\begin{aligned} W(f_c, g_c) & \approx W(0, 0) = 1 \\ W(\pm f_m + f_c, g_c) & \approx W(\pm f_m, 0) \end{aligned} \quad (18)$$

The first-order spectrum of intensity is thus simplified as:

$$I(nf_m, 0) = C_0 S \exp\{jk[W(f_m, 0) - W(0, 0)]\} + C_0 S \exp\{jk[W(0, 0) - W(-f_m, 0)]\} \quad (19)$$

It is obvious to note that the simplifications in Eq. (18) are the crucial reason to cause measurement errors. The first-order spectrum of intensity in Eq. (17) consists of two parts, both of which are the sum of aberrations over the integral region  $S$  shown in Fig.9, while in Eq. (19) they are simplified as the aberration at the sampling point multiplied by the integral region  $S$ . As the partial coherent factor increases, this effect of aberration smoothness is more serious as the integral region  $S$  also increases, thus leads to more errors of aberration measurement.

## 5. CONCLUSIONS

In this paper, the aberration measurement technique based on AIS has been explicitly presented. Two linear models have been mathematically derived, revealing the relationships between the odd aberration and phase shift of the first-order spectrum of image intensity, and between the even aberration and defocus, respectively. The simulation work conducted by PROLITH shows that this technique achieves perfect results with nearly fully coherent illumination, but the absolute measurement error becomes larger with the partial coherent factor increasing. Two effects of the partially coherent illumination, namely effect of diffraction spot and effect of aberration smoothness have been proposed to interpret such influence. It is demonstrated that this technique only works best with coherent sources, and is therefore unsuitable for aberration measurement in conventional lithographic tools with partially coherent illumination. In order to achieve higher measurement accuracy, this technique should be improved by further considering the influence of partial coherent factor on pupil sampling.

## ACKNOWLEDGEMENTS

This work was supported by National Natural Science Foundation of China (Grant No. 50775090), National Basic Research Program of China (Grant No. 2009CB724204), National Hi-Tech Research and Development Program of China (Grant No. 2006AA04Z325), and Program for New Century Excellent Talents in University of China (Grant No. NCET-06-0639). The authors would like to thank National Engineering Research Center for Lithographic Equipment of China for supporting this work and KLA-Tencor Corporation for providing an academic usage product of PROLITH™ software.

## REFERENCES

- [1] Smith, B. W. and Schlieff, R., "Understanding lens aberration and influences to lithographic imaging," Proc. SPIE 4000, 294-306 (2000).
- [2] Wang, F., Wang, X. and Ma, M., "Measurement technique for in situ characterizing aberrations of projection optics in lithographic tools," Appl. Opt. 45, 6086-6093 (2006).
- [3] Zernike, F., "Beugungstheorie des Schneidenverfahrens und seiner verbesserten form, der Phasenkontrastmethode," Physica 1, 689-704 (1934).

- [4] Ma, M., Wang, X., and Wang, F., "Aberration measurement of projection optics in lithographic tools based on two-beam interference theory," *Appl. Opt.* 45, 8200-8208 (2006).
- [5] Van de Kerckhof, M., de Boeij, W., Kok, H., et al, "Full optical column characterization of DUV lithographic projection tools," *Proc. SPIE* 5377, 1960-1970 (2004).
- [6] Fujii, T., Suzuki, K., Mizuno, Y. and Kita, N., "Integrated projecting optics tester for inspection of immersion ArF scanner," *Proc. SPIE* 6152, 615237 (2006).
- [7] Fujii, T., Kougo, J., Mizuno, Y., et al, "Portable phase measuring interferometer using Shack-Hartmann method," *Proc. SPIE* 5038, 726-732 (2003).
- [8] Ohsaki, Y., Mori, T., Koga, S., Ando, M., et al, "A new on-machine measurement system to measure wavefront aberrations of projection optics with hyper-NA," *Proc. SPIE* 6154, 615424 (2006).
- [9] Van der Laan, H., Dierichs, M., Van Greevenbroek, H., et al, "Aerial image measurement methods for fast aberration setup and illumination pupil verification," *Proc. SPIE* 4346, 394-407 (2001).
- [10] Tyminski, J. K., Hagiwara, T., Kondo, N. and Irihama, H., "Aerial image sensor: in-situ scanner aberration monitor," *Proc. SPIE* 6152, 61523D (2006).
- [11] Higashibata, S., Hagiwara, T., Mizutani, H., et al, "Aerial image sensor for self-calibration of wafer steppers," *Proc. SPIE* 4346, 1635-1643 (2001).
- [12] Tsuneyuki, H., Masato, H., Naoto, K., Kosuke, S., et al, "Self calibration of wafer scanners using aerial image sensor," *Proc. SPIE* 4691, 871-881 (2002).
- [13] Hagiwara, T., Kondo, N., Hiroshi, I., Suzuki, K. and Magome, N., "Development of aerial image based aberration measurement technique," *Proc. SPIE* 5754, 1659-1669 (2005).
- [14] Hopkins, H., "Canonical coordinates in geometrical and diffraction image theory," *Jpn. J. Appl. Phys.* 4, 31-35 (1965).
- [15] Nakashima, T., Slonaker, S. D., Kudo, T. and Hirukawa, S., "Evaluation of Zernike sensitivity method for CD distribution," *Proc. SPIE* 5040, 1600-1610 (2003).
- [16] Hiroshi, N., Takashi, S., "Techniques for measuring aberrations in lenses used in photolithography with printed patterns," *Appl. Opt.* 38, 2800-2807 (1999).